From ERATO Basic Research to the Blue EdgeTM Rotor Blade: an Example of Virtual Engineering ?

Philippe Beaumier, Berend G van Der Wall, Kurt Pengel, Christoph Kessler, Marc Gervais, Yves Delrieux, Jean-François Hirsch, Pascal Crozier

From ERATO Basic Research to the Blue Edge™ Rotor Blade: an Example of Virtual Engineering?

Philippe Beaumier
Deputy Director
Applied Aerod. Dept.
ONERA
Meudon, France

Christoph Kessler
Rotorcraft Branch Head
DLR
Braunschweig, Germany

Yves Delrieux
Research Engineer
ONERA
Chatillon, France

Berend G. van der Wall
Senior Scientist
DLR
Braunschweig, Germany

Marc Gervais
Head Aerodynamics
& Performance
Airbus Helicopters
Marignane, France

Jean-François Hirsch
Overall Blade Design
Airbus Helicopters
Marignane, France

Kurt Pengel
Project Engineer
DNW
Emmeloord, Netherlands

Pascal Crozier
Project Engineer
Wind-Tunnel Dept.
ONERA
Modane, France

ABSTRACT

In 2015, Airbus Helicopters unveiled the secrecy around its Dauphin successor and presented the all new H160 helicopter. A special feature immediately attracting attention is its unusual and revolutionary fore-aft swept main rotor blade. This design, aiming at reducing the blade-vortex interaction noise signature and also reducing fast forward flight power requirements, finds its origins far back in the 90s, when DLR and ONERA formed a joint team to acoustically optimize a rectangular reference rotor blade. Based on state-of-the-art comprehensive rotor codes and a 50-50 work share, the ERATO rotor blade design was developed, patented worldwide and tested on a rotor test rig and in the wind tunnel. Airbus Helicopters took up that design, optimized hover and forward flight high lift performance and prepared it for serial production, until it finally made it as the Blue Edge™ rotor blade on the H160 helicopter. The paper covers the history and technical achievements, wind tunnel test results and flight tests.

NOTATION

a_∞	Speed of sound, m/s
bpf	Blade passage frequency, multiples of N_b/rev
c	Airfoil chord, m
C_n	Normal force coeff., $C_n = 2L'/(\rho_\infty c V^2)$
C_p	Pressure coefficient, $C_p = 2(p - p_\infty)/(\rho_\infty V^2)$
C_P	Power coefficient, $C_P = P/(\rho_\infty \pi R^2 (\Omega R)^3)$
C_P^*	Power coefficient, based on Ω^*
C_T	Thrust coefficient, $C_T = T/(\rho_\infty \pi R^2 (\Omega R)^2)$
C_W	Weight coefficient, $C_W = W/(\rho_\infty \pi R^2 (\Omega R)^2)$
C_W^*	Weight coefficient, based on Ω^*
L'	Section lift per unit span, N/m
M	Mach number, $M = V/a_\infty$
M_h	Hover tip Mach number, $M_n = \Omega R/a_\infty$
N_b	Number of blades
p_∞	Steady pressure
P	Power, kW
P_b^*	Power coefficient, based on Ω^*, $P_b^* = 200\, C_P^*/\sigma$
R	Rotor radius, m
T	Rotor thrust, N
V	Relative velocity at a blade element, m/s
V_∞	Wind speed, true air speed, m/s
W	Virtual model weight force, N
α_S	Shaft angle of attack, deg
γ	Flight path angle, deg
Γ_b	Blade element circulation, $\Gamma_b = L'/(\rho V)$, m²/s
μ	Advance ratio, $\mu = V_\infty \cos\alpha/(\Omega R)$
μ^*	Advance ratio, based on Ω^*
ρ_∞	Air density, kg/m³
σ	Rotor solidity, $\sigma = N_b c/(\pi R)$
ψ	Rotor blade azimuth angle, deg
Ω	Rotor rotational speed, rad/s
Ω^*	Reference rotational speed, 100 rad/s

Presented at the Rotorcraft Virtual Engineering, Liverpool, 8-10 Nov. 2016. First presented at the 72nd Annual Forum & Technology Display

AH	Airbus Helicopters
AHS	American Helicopter Society International
BVI	Blade Vortex Interaction
DGAC	Direction Générale de l'Aviation Civile
DLR	Deutsches Zentrum für Luft- und Raumfahrt e.V. (German Aerospace Center)
DNW	Deutsch-Niederländische Windkanäle (German-Dutch Wind Tunnels)
EASA	European Aviation Safety Agency
ERATO	Etude d´un Rotor Aéroacoustique Technologiquement Optimisé (Aeroacoustically opt. rotor)
EMS	Emergency Medical Service
EPN	Effective Perceived Noise Level
FCM	Fringe Correlation Method
ICAO	International Civil Aviation Organization
LLS	Laser Light Sheet
MBB	Messerschmitt-Bölkow-Blohm
MTOW	Maximum Take-Off Weight
ONERA	Office National d'Etudes et Recherches Aérospatiales (The French Aerospace Lab)
PIV	Particle Image Velocimetry
SPA	Strain Pattern Analysis

INTRODUCTION

Since the early developments of rotary wing aircraft in the late 19th century, the first flight in 1907, and a period of maturation during 1920 to 1945, helicopters have made tremendous progress in performance, handling qualities, comfort, reliability, and efficiency. Some additional features make helicopters especially useful for many missions, which to date cannot be performed by any other contemporary series production aircraft. These include their capabilities to hover, to climb or sink vertically or almost vertically, to fly slowly in any horizontal direction (even backwards), and still maintain good handling qualities and manoeuvrability. This is why helicopters have conquered their niche in the aircraft market.

These advantages, but also their relatively small outer dimensions (i.e. their footprint), allow helicopters to fly at low altitudes within an obstacle backdrop and land almost everywhere even in confined areas. Despite the undoubtedly increased maturity of helicopters, some challenges still remain like high noise levels, high vibration levels, high demands on hover figure of merit and high speed forward flight, and hence limited capabilities in terms of maximum speed and range. While most of the above mentioned drawbacks of helicopters are of concern for the crew (e.g. high vibration level) and operators (e.g. limited speed and range), this is different for the noise radiated by helicopters.

Helicopters often operate at low altitudes and close to populated areas, e.g EMS helicopters which land on or next to hospitals in cities, see Ref. 1. This fact and the high noise level themselves have a direct impact on the annoyance of the population on the ground, (Ref. 1, 2), and might hinder acceptance or even increase of helicopter operation in proximity to populated areas even for well accepted EMS missions. Mooreman has documented the impact of increasing helicopter operations and the decreasing acceptance of the public due to noise issues for large cities like the Los Angeles County (Ref. 3), Long Island, and Chicago (Ref. 4), but also for US national parks (Ref. 5).

Therefore, low noise emissions of helicopters are mandatory (Ref. 1, 6). This need is also documented by the initiation of the Noise Initiative by AHS International[1]. The following noise sources contribute to the total helicopter noise (Ref. 6):

- main rotor:
  - thickness and loading noise,
  - blade vortex interaction (BVI),
  - high speed impulsive noise,
  - blade wake interaction,
  - trailing edge noise,
- tail rotor (same as for main rotor and in addition interaction with body and main rotor wakes),
- engines, (compressor, turbine, combustion),
- and airframe (fuselage, skids).

While BVI is of more concern during descent or maneuvering flight (Ref. 7, 8), thickness and loading noise are of general importance during all flight segments. Both, BVI noise and high speed impulsive noise show an impulsive character at high levels (Ref. 8). The impulsive noise is very annoying, since it dominates the noise emission in the mid-frequency range to which human subjective response is very sensitive (Ref. 7). For BVI occurrence in descent, this is all the worse, since in this flight segment the helicopter gets closer to the ground and hence closer to the population (Ref. 1).

The BVI phenomenon is caused by unsteady pressure fluctuations on the rotor blades (Ref. 8, 9). These fluctuations result from interactions of a blade with vortices generated by preceding blades. The responsible surface pressure fluctuations are concentrated mainly at the blade's leading edge (Ref. 8) and at the blade tip. Experiments have shown that two BVI locations occur in descent flight condition: one on the advancing side in the first quadrant of the rotor disc, the other one on the retreating side in the fourth quadrant (Ref. 7, 10).

The noise has a strong directivity characteristics, which is mostly forward and below the rotor plane. Due to this, pilots are in most cases unaware of the noise emission and

[1] https://vtol.org/what-we-do/noise-initiative

the considerable community annoyance they are causing (Ref. 8). Maximum noise levels of helicopters are defined by the International Civil Aviation Organization (ICAO) in Ref. 11, Annex 16, and most of the helicopters certified by the European Aviation Safety Agency (EASA) are certified in takeoff, overflight (i.e. horizontal flight), and approach according to Chapter 8 of Ref. 11, see Ref. 12. Allowed levels are shown in Figure 1. A summary on helicopter related noise issues and their relevance to a community is given by Leverton and Pike (Ref. 13).

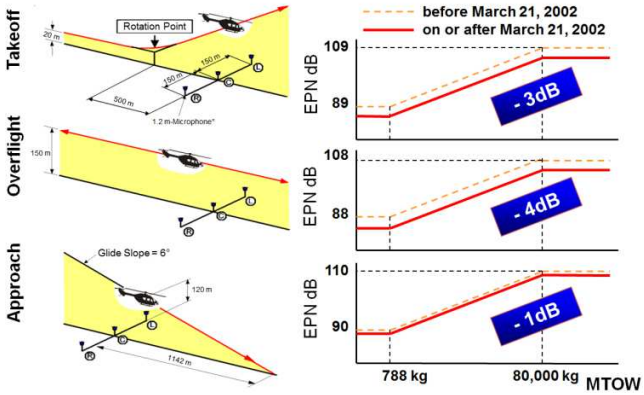

Figure 1: ICAO noise certification limits of Annex 16, Volume I, Chapter 8.

According to this, the reaction of the public to helicopters dependent on several factors, some of which are completely unrelated to the maximum helicopter noise level. The subjective character of the sound is equally or more important than the absolute noise level itself, which seems to contradict the stipulation of maximum noise levels. Improvements should not only focus on the reduction of the noise level itself, but also on reducing the impulsive character of the noise. This would lead to greater acceptance in the public.

Recommendations given in Ref. 13 include a reduction of main and tail rotor tip speeds, usage of thin blade profile sections, low noise blade tips, increased number of blades, etc. For older helicopter designs it is being recommended to fly at higher heights above the ground and use noise abatement procedures for normal operations. Also, these helicopters should not fly at very high speeds in order to minimize high-speed impulsive noise intensity and exposure time.

Two mechanisms are addressed in Ref. 13 to reduce the noise emissions of helicopters: the first one is related to passive helicopter design aspects, the second one to helicopter operations. Some of these noise related helicopter design aspects are already used at modern helicopters. How well passive improvements can reduce noise emissions is shown in Figure 2. For selected turbine powered helicopters which have been certified according to chapter 8 and which have a MTOW of 1 to 6 to this figure shows noise values in approach in comparison to the permissible noise levels. Both limits of Figure 1 have been included in the figure. In contrast to those shown in Figure 1, they are no straight lines, since a linear MTOW-axis has been used for Figure 2 to allow for a better separation of the data points. For the data points of Figure 2 it has not been distinguished whether helicopters have to fulfil the strong new limits or the somewhat relaxed older ones. This difference is for residents in the vicinity of helicopter operations actually of minor importance. Noteworthy is the No Tail Rotor System (NOTAR) design installed on the MD902 (Ref. 14), but noise radiation could also be reduced by flight procedures as demonstrated on DLR's EC135 test aircraft, Ref. 15.

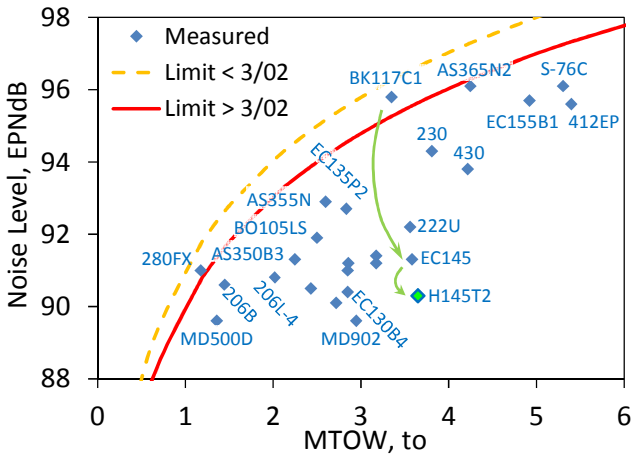

Figure 2: Measured noise levels and ICAO limits of various helicopters during approach, data: Ref. 12.

In addition to the above mentioned passive noise reduction, active rotor control can contribute to a significant noise reduction (5 to 6dB), but would increase system complexity of helicopters. It can additionally reduce vibrations or power consumption in high speed forward flight. A survey on various technologies has been given e.g. in Refs. 6, 16, and 17. ONERA experience in active flap technology can be found in Refs. 18 and 19.

In the future, even stronger noise certification requirements are foreseeable. This and the in general negative aspect of noise emission by aircraft in the public both motivate research establishments and manufacturers to address further noise reduction technologies. An overview on current noise reduction activities at US and European helicopter manufacturers is given in Ref. 14. An overview on various blade design programs with the intention to reduce BVI noise is given in Ref. 8. However, it is being mentioned that not all projects focusing on the blade tip design were successful. Some could simply not reduce BVI noise, others generated high control loads or even showed power penalties.

How well proper blade design can reduce noise while also showing power benefits has been demonstrated in a joint ONERA-DLR research program called ERATO (Etude d´un Rotor Aéroacoustique Technologiquement Optimisé), see Ref. 20. This research project especially has targeted the

BVI noise reduction and hence has addressed a noise source with very impulsive character which has been mentioned above. The excellent results triggered a follow-on project in order to further raise the maturity level of this technology, in which Airbus Helicopters and ONERA designed and tested a full-scale variant of the ERATO concept. Airbus Helicopters has first shown this modified ERATO blade as its Blue Edge™ design at the Heli-Expo 2010 in Houston. Now, the Blue Edge™ blade has found its way to the H160 helicopter which is currently under flight test evaluation. This paper gives an overview on both the ONERA-DLR research project ERATO and its results as well as the development activities at Airbus Helicopters.

THE ONERA-DLR ERATO PROGRAM

In 1991 ONERA and DLR formed a joint team to design a rotor blade with reduced BVI noise signature purely by passive design, leading to the ERATO rotor blade design (Refs. 21-27). Quarterly meetings took place to exchange results of parameter variations and define the actions for the next steps. Industry representatives from Aerospatiale and MBB (from 1992 on as Eurocopter; renamed in 2014 to Airbus Helicopters) joined the meetings as industrial observers and contributing the design optimization with their expertise. Since the rotor was to be tested in both the German Dutch Wind tunnels Large Low speed Facility DNW-LLF on DLR's rotor test rig (December 1998) as well as in ONERA's S1MA large transonic wind tunnel (March 1998) the radius was chosen as 2.1 m and the rotational sense counter-clockwise as seen from above.

The modeling and simulation codes employed were mainly based on Blade Element Theory: the S4 isolated high resolution rotor code on DLR side, and the Airbus Helicopters R85 code further improved by ONERA, which later formed the basis of the HOST code. DLR used a prescribed wake method based on the Beddoes model while ONERA used their MESIR free-wake. The reference flight condition was a representative 6° descent condition at about 70 kts (35 m/s) flight speed and scaled-down loading. With the boundary to keep the thrust weighted solidity constant the following parameters were varied in work share with the overall goal to reduce BVI noise radiation:

- chord distribution (taper)
- quarter chord line distribution (blade sweep)
- twist distribution
- airfoil distribution
- rotor rotational speed (tip Mach number)

The starting point of the optimization process was the ONERA 7AD rotor blade geometry. The ERATO blade design freeze happened in 1996 and a Mach scaled model rotor was jointly built (Ref. 21). Figure 3 shows details of the ERATO blade design, compared to the 7AD rotor reference blade.

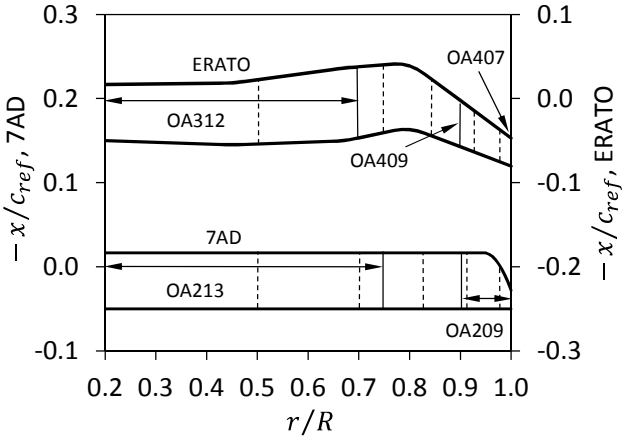

(a) ERATO rotor blade vs. 7AD reference blade geometry. Dashed: sections fully instrumented with pressure sensors.

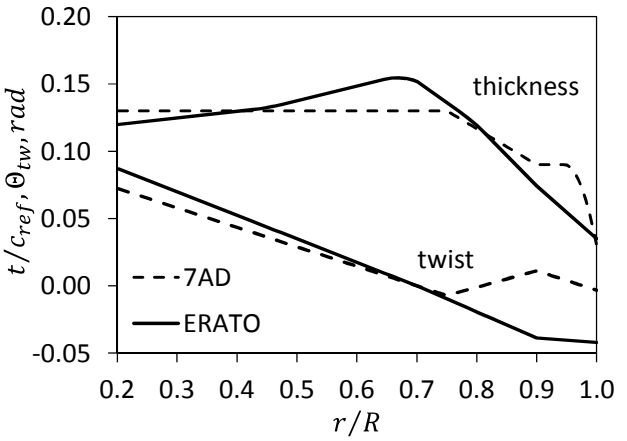

(b) ERATO and 7AD blade twist and absolute thickness.

Figure 3: ERATO aeroacoustically optimized rotor blade design compared to the 7AD reference rotor blade.

The design features of the ERATO aeroacoustically optimized blade are:

- the largest chord is located around 65% radius (leading to a strong taper towards the tip) with the goal to redistribute the lift from the tip towards more inboard, aiming at reducing the tip vortex strength;
- a combination of fore-aft sweep with the goal to distribute BVI interaction topology from a quasi-parallel BVI (7AD) to azimuthally/radially distributed BVI (ERATO);
- as a side effect, sweep reduces the effective Mach number on the blade and thus alleviates compressibility effects, leading to less power drag in high speed flight and – though no design goal – reducing rotor power consumed;
- usage of modern next generation rotorcraft airfoils with high lift capability in the inner regions up to 70% radius; combined with linear strakes to thinner and finally transonic airfoils at the blade tip with

reduced shock characteristics at high subsonic Mach numbers (again reducing drag and power);

- usage of higher twisted blades compared to the reference rotor which again aims at redistribution of lift towards more inboard locations.

Of course, the fore-aft swept blade design was suspected to generate aero-elastic problems due to strong couplings of especially flap and torsion modes, compared to a straight blade such as the 7AD. The structural design was therefore carefully chosen at least to avoid strong coupling at the nominal rotational speed. Any flap-torsion mode proximity was requested not to be close to a blade harmonic number, i.e., 4/rev or 8/rev (as the number of blades was 4) to avoid excessive vibration transmitted to the non-rotating frame. The computed fan diagram of both model-scale rotors, using a finite element beam method based on the Houbold-Brooks equations is given in Figure 4.

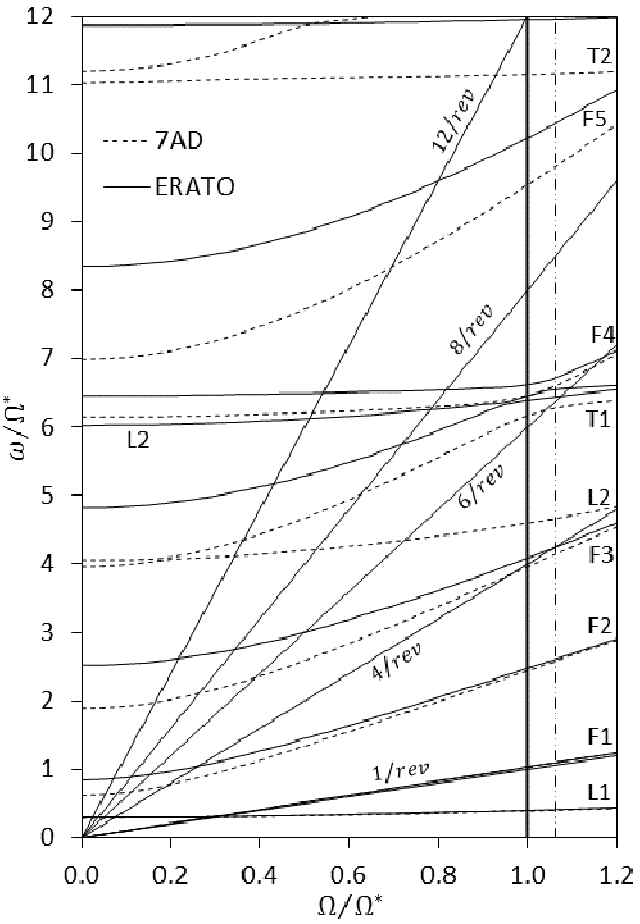

Figure 4: Fan diagram of the 7AD and ERATO blades.

While the 7AD rotor shows a proximity of the fourth flap mode to the first torsion mode close to 6/rev with the second lag mode well separated from it, the ERATO rotor has all three of them in close proximity around 6.5/rev at its nominal speed of rotation, but far away from the blade harmonics 4 and 8/rev.

Wind Tunnel Testing in DNW-LLF and S1MA

In order to get maximum use of wind tunnel tests and to understand the underlying physics, one rotor blade was heavily instrumented with 125 absolute pressure sensors and 32 strain gauges. The other blades got dummies for blade dynamics reasons and some strain gauges as well. All blades were equipped with flap, lag and pitch sensors at the articulation and pitch bearing.

The DNW-LLF tests, where in the open jet configuration about 78 m/s maximum wind speed could be achieved (Figure 5), focused on rotor acoustics, vibrations, and performance in hover and at low to moderate speeds. The S1MA tests (Figure 10) aimed at high speed flight with respect to rotor performance and noise, high lift (including stall) and vibration. DNW testing (Refs. 20, 22-23) capabilities employed in its low back-ground noise anechoic environment included a microphone traverse for measurement of the noise carpet below the rotor (centered in the lower half of Figure 5). Optical blade deformation measurements were performed by a fringe correlation method (FCM, complementary to the strain gauges readings within the blades), Ref. 24, that was provided and operated by DNW. With this method it is possible to measure flapwise and torsional deflections along the blade span at selected azimuthal angles. This technique is based on the fact that a grid, which is projected on the surface of a structure, will change its pattern when the structure is deformed or displaced.

Figure 5. The ONERA-DLR ERATO rotor mounted in the DNW LLF 8 m by 6 m anechoic open test section.

For this purpose the projection of the grid has to be executed from the opposite direction of the recording device, which was a fast motion video camera in the ERATO test campaign. By comparing the image of the non-deformed and non-displaced blade with one that is deformed and deflected, the relative deformation and displacement of the structure can be determined. The result of FCM is thus the difference of the total deflections of two rotor-conditions. Figure 6 represents a fringe pattern projected onto an ERATO blade.

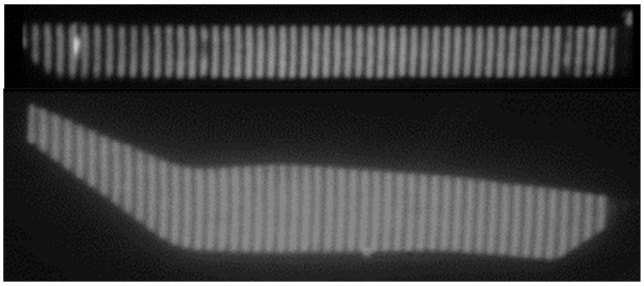

Figure 6. A Fringe Correlation pattern projected onto one of the 7AD and ERATO rotor blades.

An example result from the reference operating condition representing a 6° descent flight is shown in Figure 7. The FCM provides information of local deflections from all visible surface points of the blade, while the strain gauge measurements provide the local bending moments at the point of the sensor, and deflections of the entire blade are computed using beam bending theory with many simplifying assumptions included.

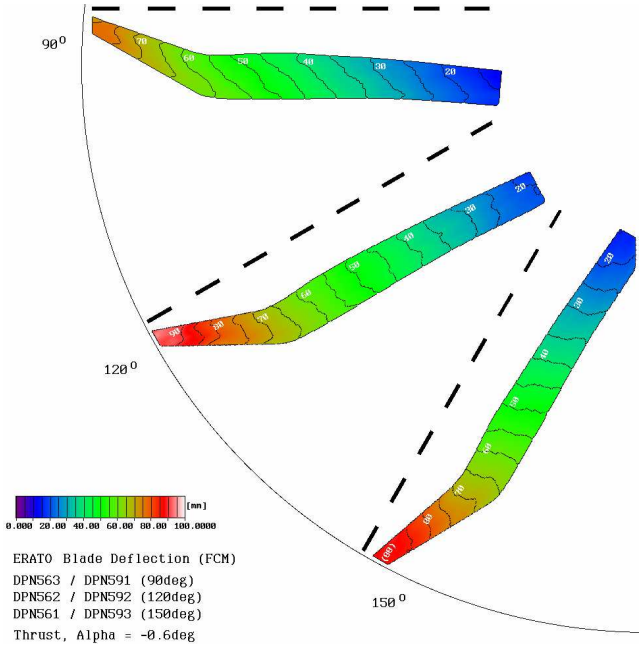

Figure 7. Vertical deflection of the ERATO blade measured at different azimuth during rotation.

In order to determine tip vortex parameters as vortex core diameter, swirl velocity and circulation, DNW provided their Particle Image Velocimetry (PIV) system for 2-D flow field measurements at pre-selected locations in the vicinity of the BVI area. DNW conducted the measurements and also performed the data analysis. Figure 8 represents two vector maps of a tip vortex cross section: one instantaneous and one averaged vector map. Tip vortex line locations and actual rotor blade locations have been measured by means of DNW's Laser Light Sheet (LLS) flow field visualization method. The results were used in order to calculate blade-vortex miss distances at rotor blade azimuths of strong BVI. Furthermore, these flow field visualization measurements have been done for getting an impression of the tip vortex trajectories while traveling downstream the rotor disk for a better understanding of the BVI noise phenomena. Figure 9 represents results gained by means of the LLS method.

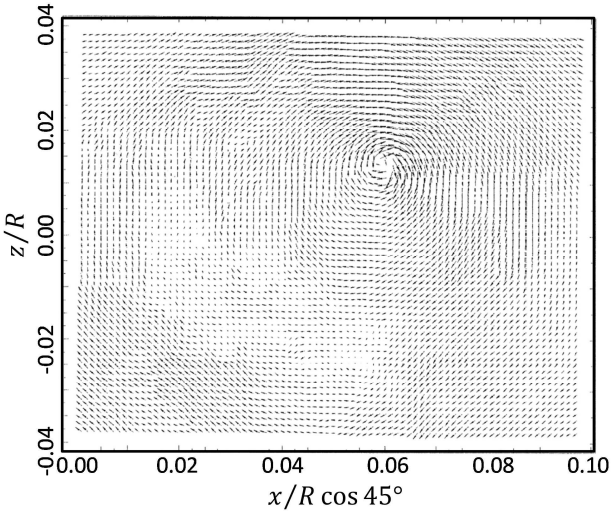

(a) Instantaneous velocity vector field

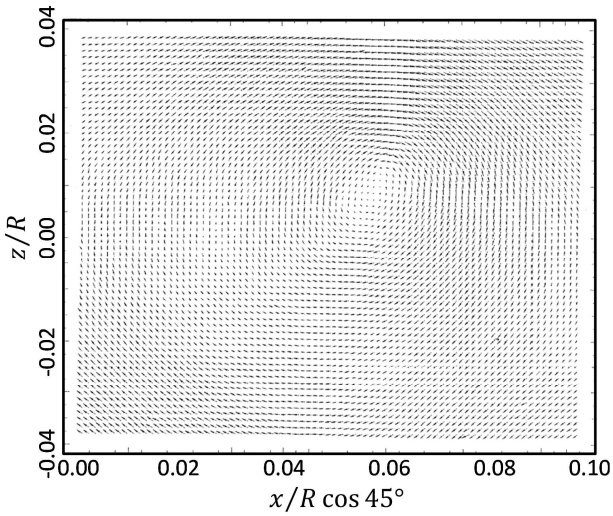

(b) Averaged velocity vector field

Figure 8. Vector maps of a tip vortex cross section measured by means of PIV.

Blade surface pressure measurements during the DNW test were performed by DLR Göttingen. 125 absolute pressure sensors were installed on the ERATO reference blade, distributed among 5 radial sections on upper and lower surface as indicated in Figure 3 (a) with additional ones located between these sections along the leading edge. The 7AD rotor had a similar number of pressure sensors, but distributed among the blades. A 6-component rotor balance was employed in all tests as part of DLR's rotor test rig with data acquired by DLR and some identical operational conditions were performed in both DNW and S1MA wind tunnels to cross-check and ensure the similarity of results.

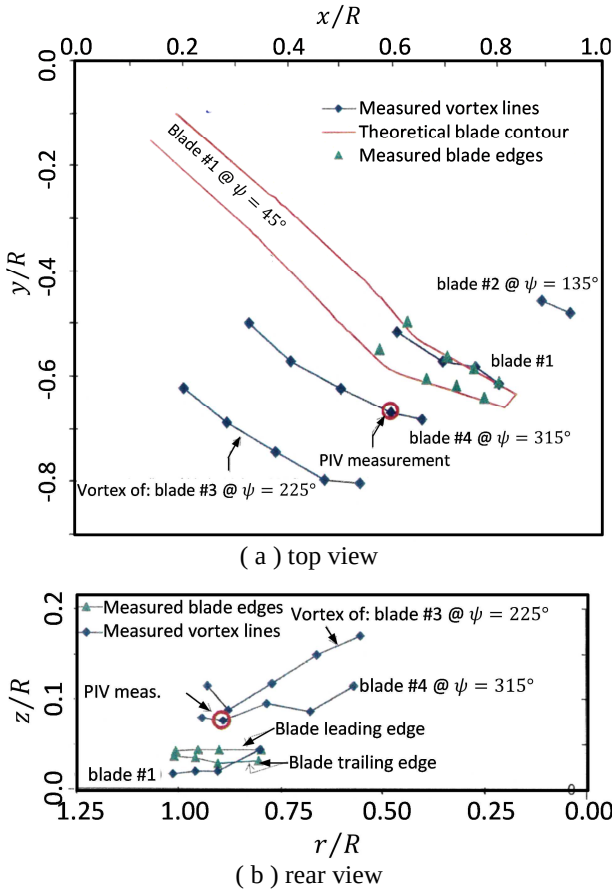

Figure 9. Tip vortex and rotor blade location measured with the LLS method. $V_\infty = 35\,m/s, \gamma = 6°$.

In S1MA, the test section was equipped with its "low speed" acoustic liners (black surfaces in Figure 10) which can withstand Mach Numbers up to 0.32. Acoustic measurements were realized using 10 microphones located especially in the area affected by BVI noise. Tests included also load measurements with a 6-component rotor balance located inside the test rig, blade deformation measurements using the Strain Pattern Analysis method (SPA), pressure measurement on the blades to establish correlation between noise levels and Mach number distribution on the blades. All data were acquired by S1MA wind tunnel operators and delivered to ONERA and DLR scientists for analysis after the test.

Wind tunnel test results

Rotor Noise Radiation

Typically for helicopters, the maximum BVI noise radiation occurs in landing approach, i.e., at flight speeds of about 70 kts (35 m/s) and 6° descent angle. In DNW-LLF a descent angle sweep from climb to steep descent was carried out to identify the maximum BVI noise radiation condition. This is shown in Figure 11 for various rotor loadings.

Figure 10. The ONERA-DLR ERATO rotor mounted in the S1MA 8 m Ø closed test section.

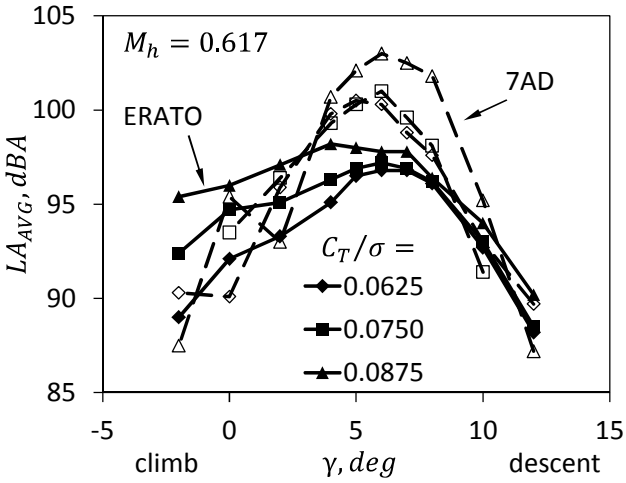

Figure 11: BVI noise reduction potential of the ERATO rotor at $V_\infty = 35\,m/s$.

At the reference 35 m/s, 6° descent condition a significant BVI noise reduction of roughly 4 dBA was demonstrated, verifying the numerical predictions, Figure 12. One of the major results of these tests was that noise could be re-

duced for a wide range of flight conditions, demonstrating a significant robustness of acoustic gains with respect to variations of descent angle, advancing velocity, trim conditions etc.

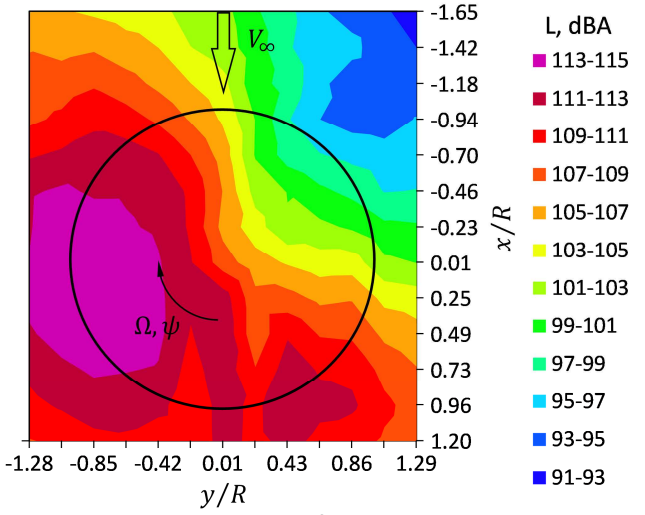

(a) 7AD reference rotor

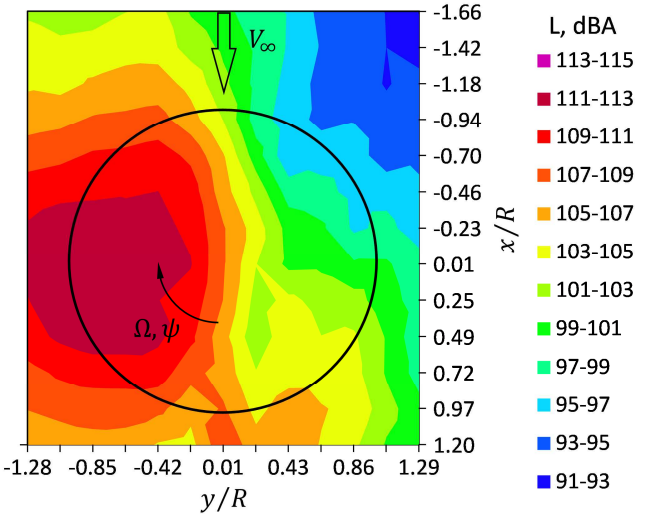

(b) ERATO rotor

Figure 12: Acoustic results of DNW-LLF tests showing the ERATO rotor with significantly less BVI noise signature compared to the straight reference blade. $V_\infty = 35\,m/s, C_T/\sigma = 0.0625, \gamma = 6°$.

The reason of BVI noise reduction was mainly seen in a different BVI topology due to the blade planform. The double sweep causes the BVI not to happen over a large radial portion simultaneously as is the case with a rectangular blade; rather it distributes the BVI event in time and space. Figure 13 (a) shows the high-frequency, BVI-related content of leading edge pressure distributions (high-pass filtered at 10/rev) as source of the noise and in (b) the same is shown for the ERATO rotor.

It can be observed in this figure in a qualitative manner that the blade pressure waves in the first and fourth quadrant of the 7AD rotor appear more intense than those of the ERATO rotor. Accordingly, the noise radiation intensity of the ERATO rotor is found significantly lower.

The source of BVI noise are high frequency loading oscillations in the first and fourth quadrant of the rotor disk, where the tip vortex axis and the blade leading edge are almost parallel to each other and simultaneously interact on a long radial part of the blade. Any noise reduction therefore is partly due to a reduction of these BVI. This is substantiated in Figure 13 for both rotors in the maximum BVI noise radiation operational condition.

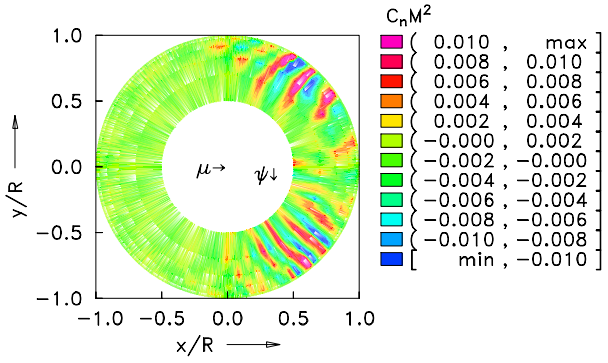

(a) 7AD rotor

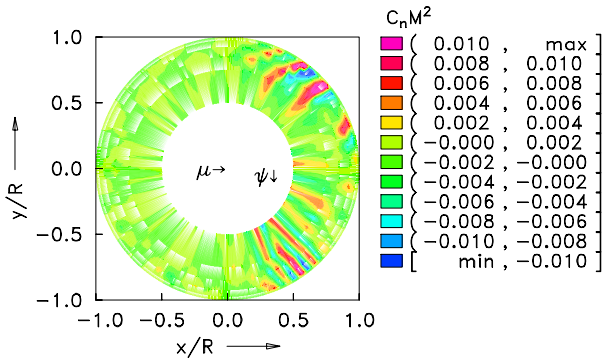

(b) ERATO rotor

Figure 13: Rotor blade loading, high-pass filtered at 10/rev, showing BVI locations and intensity. $V_\infty = 35\,m/s, C_T/\sigma = 0.0625, \gamma = 6°$.

It can be seen that the ERATO rotor has less amount of BVI in terms of number of BVI events and intensity on both the advancing side and the retreating side of the rotor. This was quantitatively confirmed by the post-treatment of LDV measurements which emphasized the reduction of the vortex intensity emitted by the ERATO blades (Figure 14). A further proof of this observation is given in acoustically relevant time derivative of the section loading at a representative radial station close to 85% radius (ERATO) and 81.5% radius (7AD) in Figure 15 (a) for the advancing side of the rotor and in (b) for the retreating side. In this case the time derivative is based on the 6-40 bpf of the data.

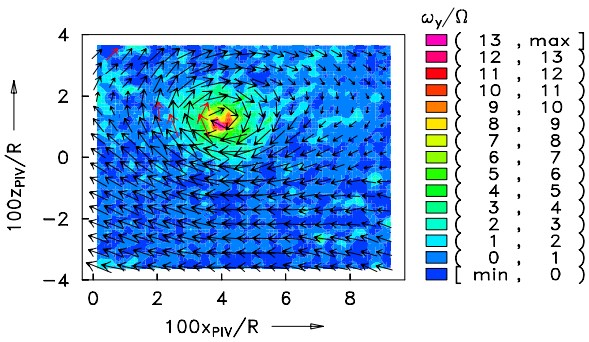

(a) 7AD rotor, $\Gamma = 4.23\, m^2/s$

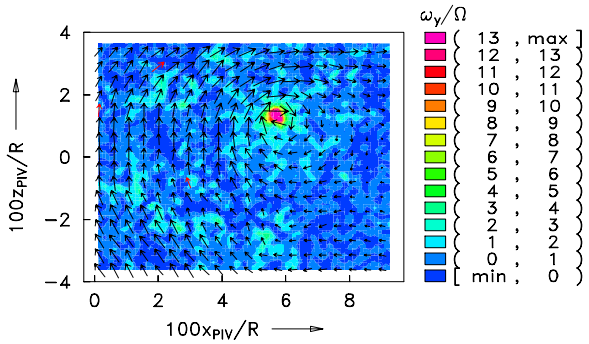

(b) ERATO rotor, $\Gamma = 3.56\, m^2/s$

Figure 14: Velocity field and vorticity ω_y derived from it around a vortex as measured by PIV.
$V_\infty = 35\, m/s\,, C_T/\sigma = 0.0875, M_h = 0.617, \gamma = 6°$

The grey shaded areas are those of parallelism of the vortex axis with the blade leading edge for a straight rotor blade. It is obvious that the 7AD rotor has stronger BVI interactions and a longer range of azimuth where the intensity is relatively large, compared to the ERATO rotor, i.e., the vortices are stronger and appear to pass the rotor blade's path in a closer manner than in case of the ERATO rotor. While the first can be explained with the blade loading at the origin of the vortex, i.e., around $\psi = 135°$ azimuth on the advancing side and around 225° on the retreating side, the latter can only be explained with a different vortex trajectory while travelling downstream across the rotor disk.

The rotor blade circulation at 135° azimuth is shown next in Figure 16, computed from the section loading. It can clearly be seen that the gradient of circulation towards the blade tip, which feeds the tip vortex, is much larger in case of the 7AD rotor than in case of the ERATO rotor. The second assumption, a different tip vortex trajectory while travelling downstream across the rotor disk, can only be due to a higher dynamic low frequency loading content in case of the ERATO rotor, compared to the 7AD. This phenomenon is known from the HART test, where this was actively controlled by means of HHC. Based on the concept of momentum theory, any additional local lift (or download) is associated with an additional downwash (or upwash) induced by it. A vortex travelling this local down- or upwash gets additional trajectory deflections.

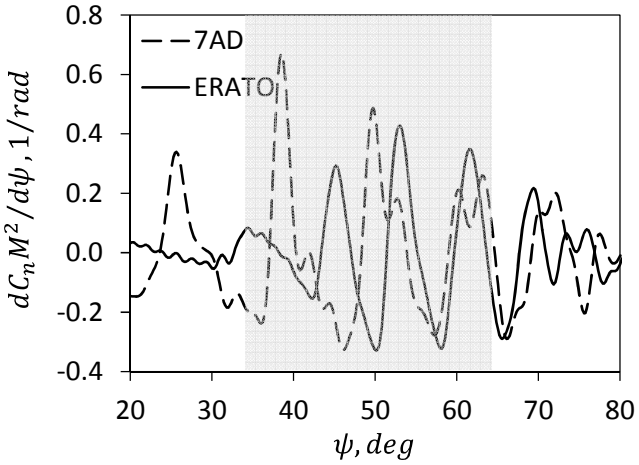

(a) Advancing side

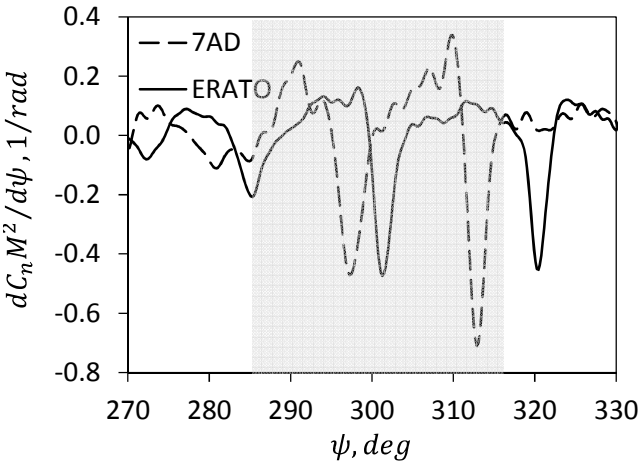

(b) Retreating side

Figure 15: Rotor blade loading, high-pass filtered at 10/rev, showing BVI locations and intensity.
$V_\infty = 35\, m/s\,, C_T/\sigma = 0.0625, \gamma = 6°$.

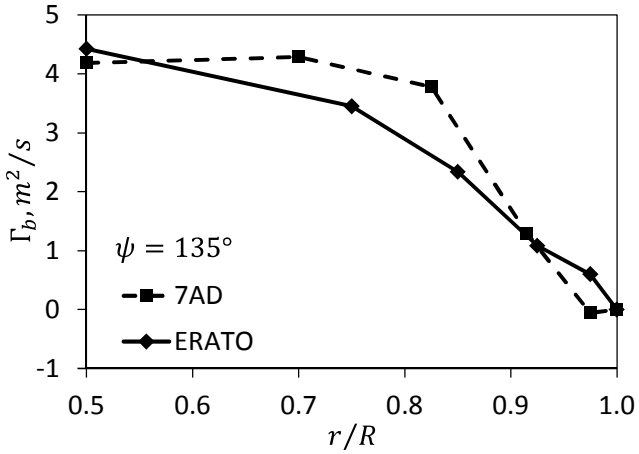

Figure 16: Instantaneous rotor blade circulation.
$V_\infty = 35\, m/s\,, \gamma = 6°$.

The low frequency content of rotor blade loading (0-10/rev) is shown in Figure 17, making proof of the assumption. While the 7AD rotor has a relatively smooth loading distribution with small to moderate harmonic content, the ERATO rotor has stronger dynamic fluctuations, quite similar to what has been observed in the HART test using HHC active rotor blade control.

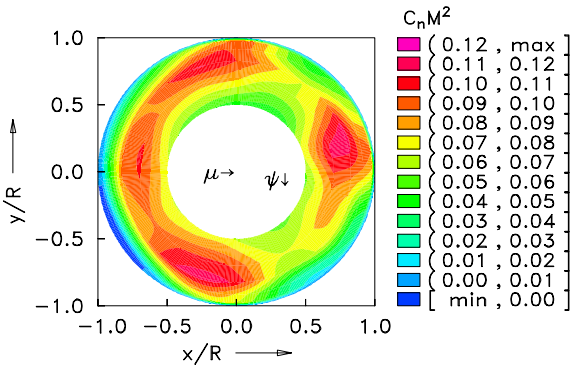

(a) 7AD rotor

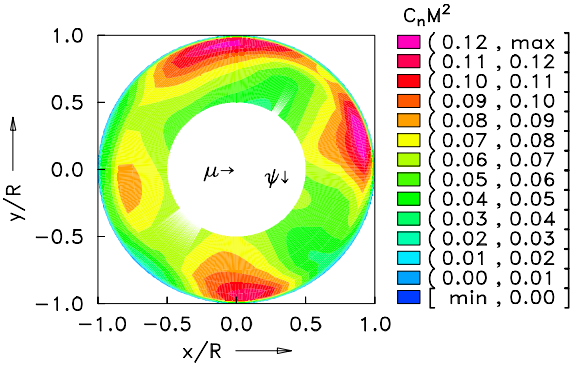

(b) ERATO rotor

Figure 17: Rotor blade loading, low-pass filtered at 10/rev. $V_\infty = 100\ km/h, \gamma = 6°$.

This was expected since due to the fore-aft swept blade shape of the ERATO blade, more flap-torsion couplings were expected from the numerical simulations during the design phase, leading to a larger dynamic content of the elastic blade deformation and thus in the lift distribution, as confirmed by the measurement of elastic deformations using the Strain Pattern Analysis (SPA) method (Figure 18).

The experiments therefore confirm a larger rotor blade dynamic motion content, leading to a larger dynamic loading content, and finally to modified tip vortex trajectories that help reducing BVI noise.

The gains in loading, thickness and transonic (high speed impulsive) noise levels were measured in S1MA wind tunnel for level flight conditions and are shown in Figure 19 where the difference between ERATO and 7AD rotor for identical operational conditions are shown. The 7AD rotor was always operated at a tip Mach number of 0.661, while the ERATO rotor was operated with different tip Mach numbers. In any condition, the rotor trim ensured the same overall lift and propulsive force for both rotors. For the same tip Mach numbers, gains are between 2 and 3 dBA, but are significantly larger with reduced tip Mach number.

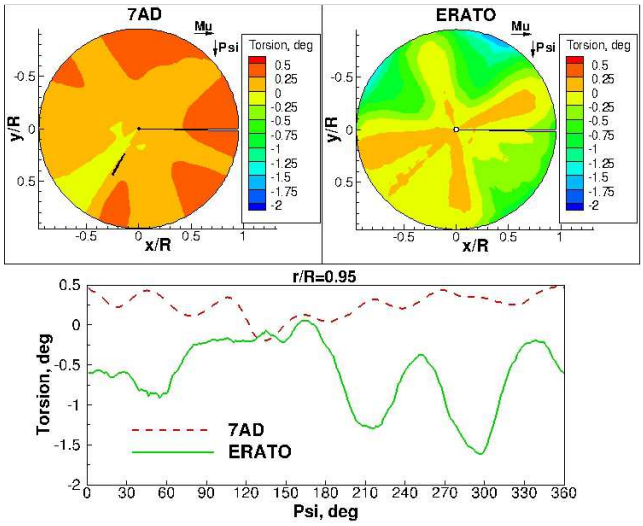

Figure 18: Torsion deformation measured by SPA method in S1MA. $M_h = 0.617, \mu = 0.283$, $C_T/\sigma = 0.075$

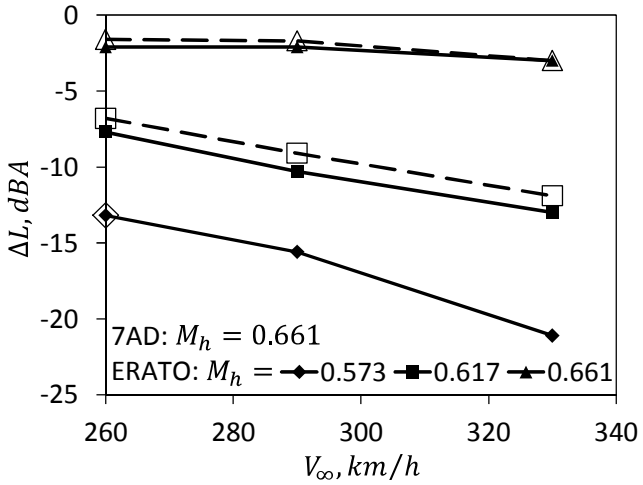

Figure 19: Gains in maximum noise levels of the ERATO rotor relative to the 7AD reference rotor in level flight. Solid: $C_T/\sigma = 0.0625$, dashed: 0.075.

The ERATO rotor is not equipped with a specifically optimized blade tip to reduce the High Speed Impulsive (HIS) noise. Nevertheless, thanks to the reduced thickness and thanks to the backward sweep, the tests have shown that the delocalization phenomenon was delayed to higher advancing speeds with the ERATO rotor (explaining the 3.5 dB reduction at 330 km/h (183 kts), Figure 19).

The influence of the rotor loading on the acoustic radiation has been analyzed. At ICAO certification flight condi-

tions (120 and 140 kts = 216 and 252 km/h), the ERATO rotor provides gains whatever the lift coefficient, up to 7 dB at $C_T/\sigma = 0.0875$ which corresponds to a strong BVI case. These tendencies were confirmed by the DNW tests as shown in the previous section. Even if the flight conditions simulated in S1MA where not those for which the ERATO design was optimized, noise reductions have been demonstrated for 75% of the measured points.

Rotor Power Consumption in forward flight

The high speed and high load tests at S1MA wind tunnel of ONERA (Refs. 20, 25) confirmed a smaller power consumption of the ERATO rotor throughout the entire range of operational conditions of up to 9% compared to the reference rotor and 5% in average, see Figure 20.

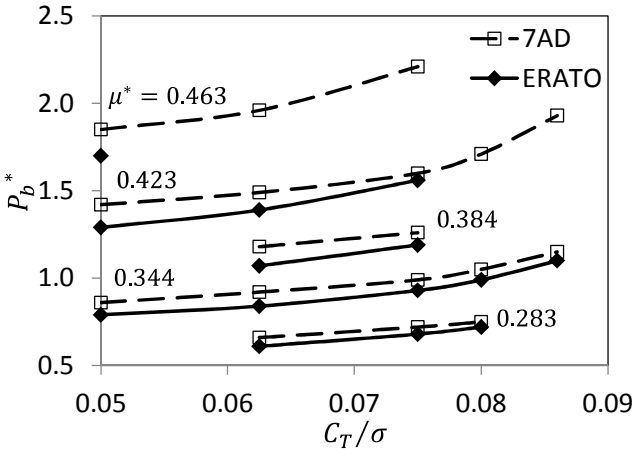

Figure 20: Power gains of the ERATO rotor.

This is mainly due to the use of new generation airfoils specifically designed for high subsonic speed conditions (OA4-OA3 series on the ERATO blade instead of OA2 series on the reference 7AD rotor blades) and to a lesser extend to the back sweep of the blade tip, reducing the compressibility effects and hence rotor power required.

The good behavior of the ERATO blade in transonic conditions is illustrated by the contours of local Mach numbers in Figure 21, extracted on-line during the S1MA tests from the measurement of the pressure distributions.

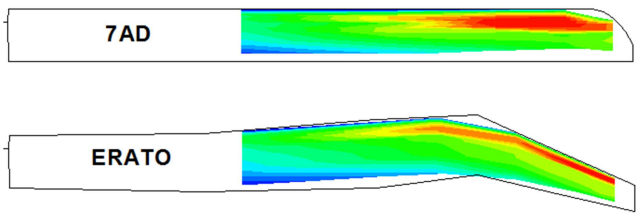

Figure 21: Measured contours of local Mach numbers on the blade on the advancing side ($\psi = 90°$) for high speed conditions in S1MA. Red: $M > 1$.

Efficiency in Hover

Although not part of the specifications given for the optimization of the rotor, hover performance assessment was done by Airbus Helicopters. The same 7AD and ERATO rotor models as used in DNW-LLF and S1MA were installed on the Marignane test rig, and the Figure of Merit of the two rotors was measured for different tip Mach numbers. A sample result of these measurements is illustrated in Figure 22. Both rotors show similar performance for thrust coefficients $C_T/\sigma < 0.087$, with even slightly higher efficiency for the ERATO rotor than for the 7AD rotor.

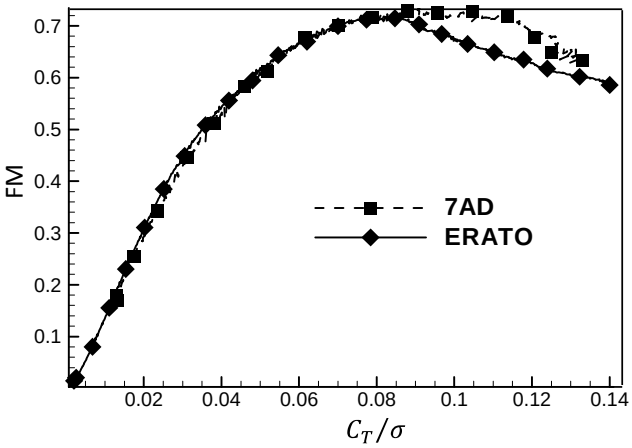

Figure 22: Measured hover performance of 7AD and ERATO rotors. $M_h = 0.617$

However, beyond $C_T/\sigma \approx 0.087$, there is a sudden loss of efficiency of the ERATO rotor, whereas the 7AD reference rotor continues to maintain efficiency higher than 0.71 up to $C_T/\sigma \approx 0.115$. This poor performance at high thrust of the ERATO rotor clearly indicated a premature stall of the blade which was not anticipated during the design phase, but was identified as a major topic to be addressed for future improvements of the rotor performance.

SHANEL AND SHANEL-L (2009-2012) CALCULATIONS AND DEVELOPMENTS ON ERATO CASES

The optimization process used for the ERATO design was based on sets of comprehensive codes. In parallel, the CFD-CAA capabilities available at ONERA have been developed and improved. In particular, the CFD capabilities to well capture the emitted vortices and more challenging to be able to properly model their characteristics from their emission up to the azimuths of interaction have been developed in the frame of the CHANCE (2001-2006) and SHANEL and SHANEL-L (2009-2012) programs.

In the framework of the French-German CHANCE cooperation, Chimera techniques have been developed and used for automatic mesh generation and adaptation in the

elsA solver. In 2004, these methods have been applied to the HART Baseline test-case, but no BVI was simulated due to too coarse blades and background grids. In the framework of SHANEL, the objectives were to capture the blade-vortex interaction with fine reference meshes and to improve the efficiency of the computations by applying recent numerical methods (high-order schemes, vorticity confinement, etc.). The simulations, using a loose CFD-CSD coupling were then applied to the complex geometry of the ERATO blades. The CFD results were used as input data for the noise analysis and compared to the HART experimental measurements.

One of the objectives was to test the efficiency of the Vorticity Confinement (VC) technique previously validated using the HART II database. The CFD were performed with the elsA code (weakly coupled with the HOST code) to solve the 3D URANS (Unsteady Reynolds-Averaged Navier-Stokes) and the acoustic predictions were made using the Ffowcs Williams-Hawkings KIM code (Ref. 32). As shown in Figure 23, the impulsive nature of BVI events is much better reproduced by the CFD simulations using the Vorticity Confinement (VC) technique, because it better preserves the vorticity of the vortices from their emission up to the interaction azimuths with a moderate number of mesh points (24 M).

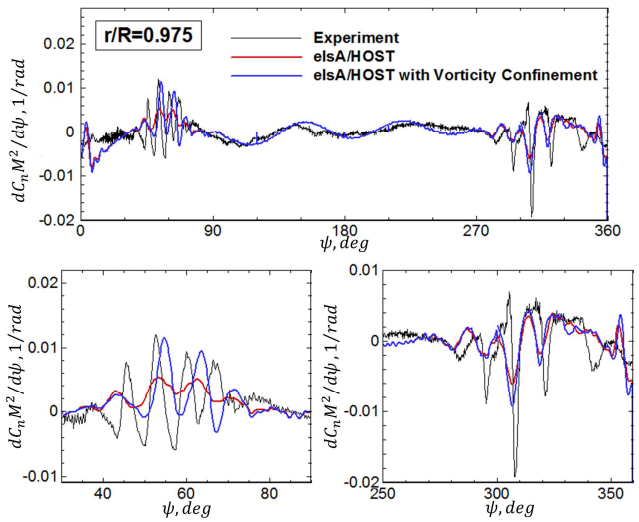

Figure 23: Measured azimuthal derivatives of section loads compared to numerical simulation.

As a consequence, noise predictions using as an input the VC results are in much better agreement with measurements, as shown by Figure 24.

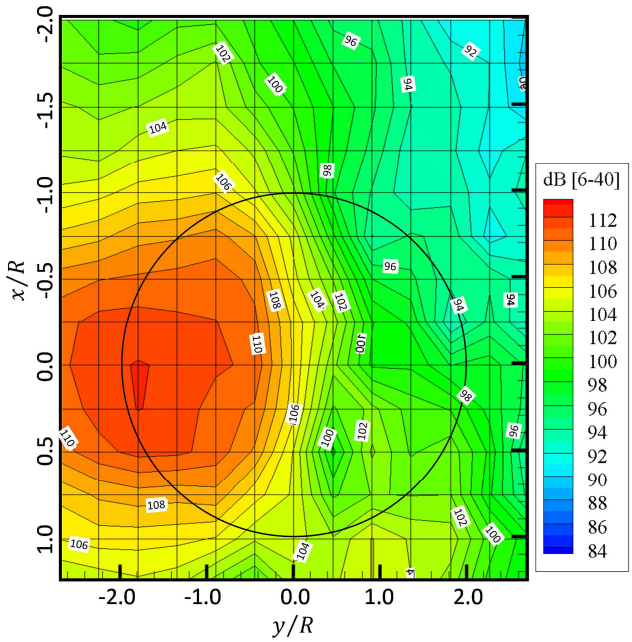

(a) Experiment

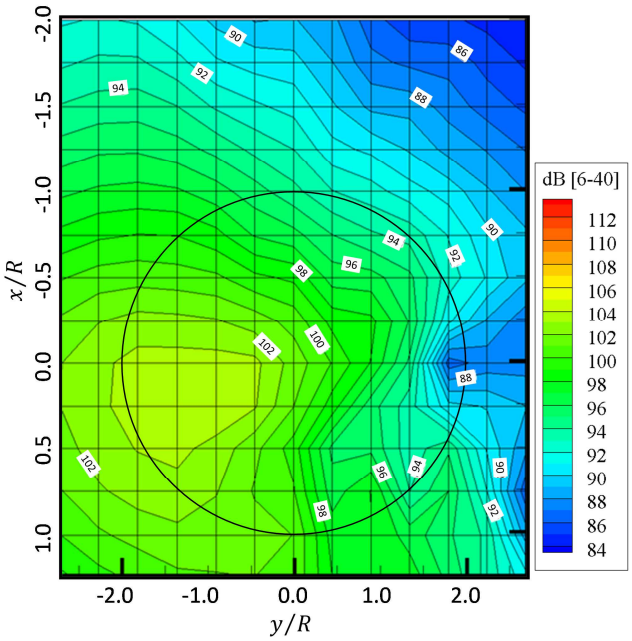

(b) *els*A KIM without VC

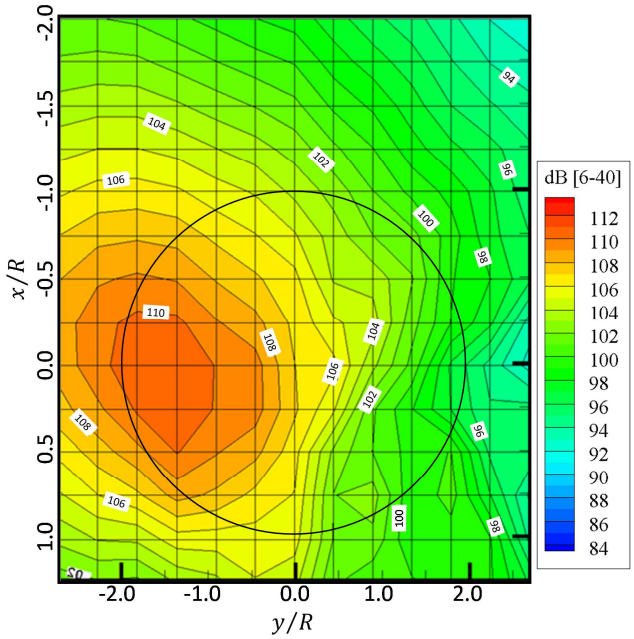

(c) *els*A KIM with VC

Figure 24: Measured BVI noise contours compared to numerical simulation.

FULL SCALE ADAPTATION AND DESIGN: FROM ERATO TO BLUE EDGE™

Following the ONERA-DLR ERATO project, a new project was launched in year 2000 on the French side with Airbus Helicopters and ONERA as acting partners in order to take benefit of the acoustically optimized ERATO blades with the objective of developing a full-scale prototype rotor. The project was subdivided into four major phases, providing clear progression and knowledge capitalization during each phase, Ref. 31. The four phases were:

- Phase 1: Selection of candidates. Starting from lessons learnt with ERATO project, a design phase was launched in order to significantly improve the hover performance and some observed dynamic behaviour. Numerical simulations in aerodynamics, acoustics and dynamics were mainly used in this optimization loop in order to select the candidate which offered the best compromise between all these significant objectives.
- Phase 2: Technology and structural design. After the selection of a candidate, the team was fully in a position to launch the structural design, dynamics optimization, strength assessment, detailed design and manufacturing tools.
- Phase 3: Validation of the design. Manufacturing began in this phase, followed by ground demonstration tests in order to validate the design and to obtain the flight clearance for the rotor.
- Phase 4: Flight demonstration on a H155 demonstrator in order to validate the aerodynamic, acoustic and dynamic characteristics and performance.

A dedicated team was created with representatives from each key area through which the blade would ultimately be designed, manufactured and tested. This multi-disciplinary approach gave wider joint ownership to the team and stimulated a creative spirit, which was necessary during certain critical phases of such an innovative design. The project was also the right platform to implement a range of simulation and design tools which could later be applied to other applications.

During the first phase of this project, the challenge at the beginning of the design phase was to propose blade shapes featuring the fore-aft sweep concept of the ERATO rotor promising for acoustics, while significantly improving the hover performance in terms of Figure of Merit. Thanks to the use of CFD for the first time in a helicopter rotor design exercise, the poor behavior in hover of the ERATO rotor could be explained and attributed to premature stall on the outboard blade sections located in the aft part of the blade, where the chord length of the aerodynamic sections were too small (Figure 25). CFD could reproduce the impact of the premature stall on the rotor performance, as demonstrated by Figure 26.

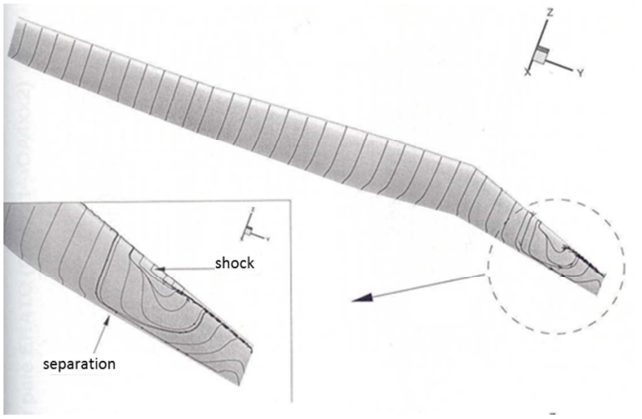

Figure 25: ERATO rotor stall in hover (CFD prediction)

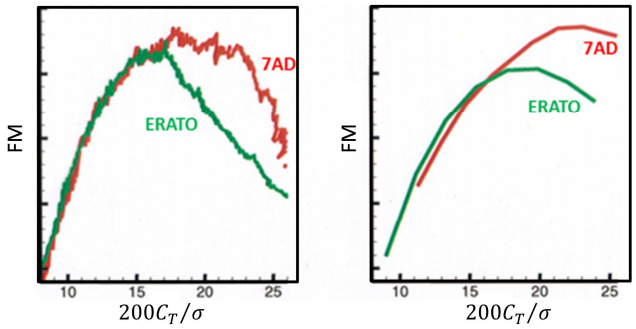

(a) Experiment (b) CFD

Figure 26: Validation of CFD method for predicting the hover performance of 7AD and ERATO rotors

This validation gave confidence in the available numerical tools to achieve the objectives of the project. As a first step, five candidate rotors were proposed, all with increased chord values on the outer part of the blade, and numerically evaluated in hover conditions, using as a reference the C0 rotor designed by Airbus Helicopters, Figure 27.

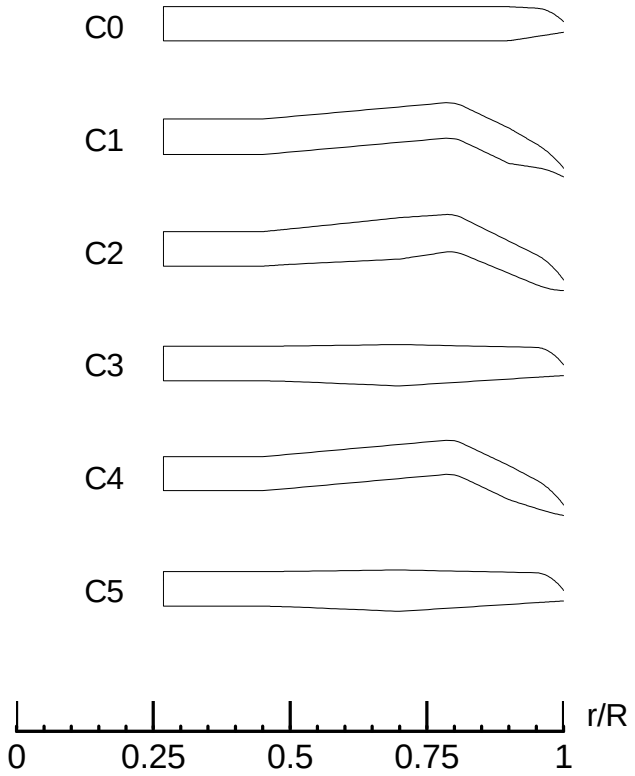

Figure 27: Initial blade shapes evaluated in hover conditions (C0 = reference)

The result of these computations, as is illustrated in Figure 28, was that all proposed candidates showed improved performance compared to the C0, with a maximum FM improvement by approximately 3 counts.The detailed investigation of the origin of the gains concluded that FM improvement came from the increased twist distribution and from the anhedral put at the blade tip which was absent on the C0 blade. Following this first step, the C4 candidate was selected and an optimization of its tip shape was carried out. It has to be highlighted here that this was the first time that a CFD solver was introduced by ONERA and Airbus Helicopters in an optimization loop to design a rotor blade.

The optimizer could modify the twist and anhedral law of the blade tip ($r > 0.9R$), using as a cost function the maximum FM. Several designs came out from the optimization runs, each featuring improved hover performance, the selection being finally made outside the optimization loop based on the noise radiated by the rotor in typical descent flight conditions, using the ONERA 'HMMAP' aero-acoustics chain (Ref. 27): this led to the so-called C4P-OPT candidate.

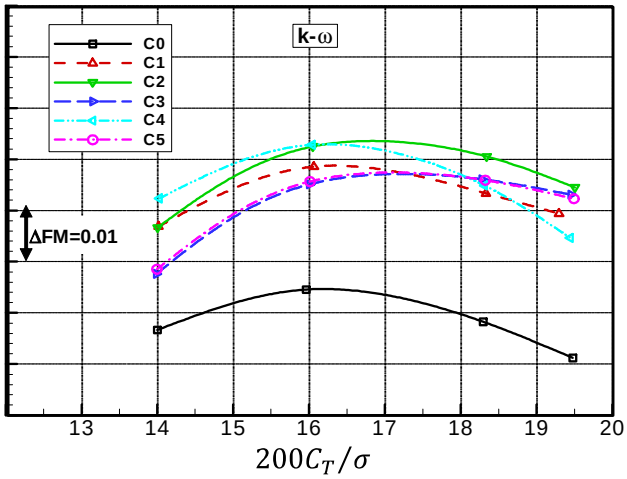

Figure 28: CFD evaluation of initial blade designs in hover conditions

Since all the optimizations carried out in this first phase of the design were done using a rigid blade assumption, the next phase was to define blade structural data and repeat the aerodynamic and acoustic simulations using the soft blade assumption. Taking into account the elastic blade deformations did not significantly modify the good hover performance of the optimized blade, but led to reduced acoustic gains (but still significant for descent angles higher than 6°, see Figure 29).

At that step of the project, the main issue was related to torsion deformations and control loads, which were found to be too high in high-speed forward flight. The best way to reduce the torsion deformations - which were mainly due to bending-torsion coupling resulting from the fore-aft sweep concept - was to try to modify the sweep angles of the blade. Since the radiated noise in descent flight is highly sensitive to this parameter, reaching a good compromise between acceptable torsion deformations and promising noise reduction was a real challenge.

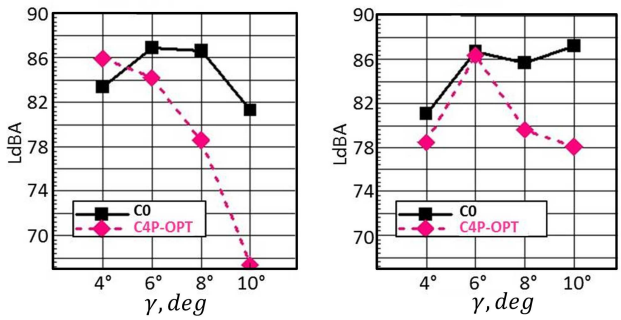

Figure 29: predicted noise levels in descent flight: influence of blade deformations, $V_\infty = 40\ m/s$.

In this phase, the main modifications brought to the design were the following: the sweep angles were changed on

the final Blue Edge™ design and the spanwise extension of the backward swept part of the blade was reduced. This led to a good aerodynamic-acoustic-dynamic compromise (Figure 30), with high expected FM in hover, and promising noise reductions in low-speed descent flight.

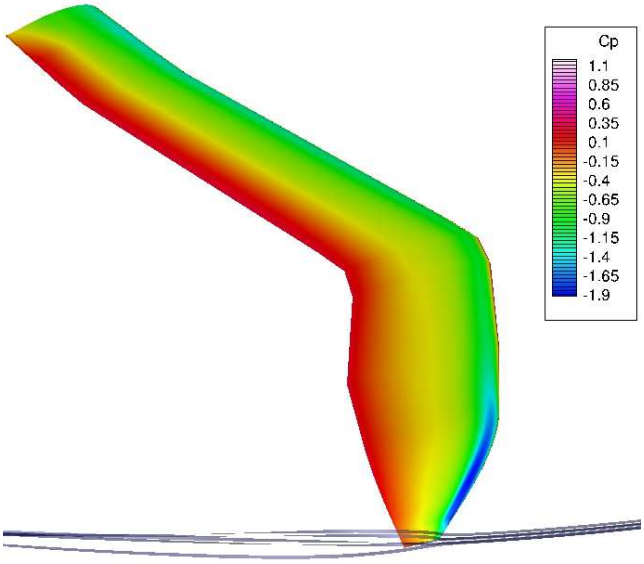

Figure 30: Blue Edge™ optimized blade with surface pressure coefficient distribution in hover.

An assessment of the flight conditions for which the Blue Edge™ design was acoustically efficient was numerically done and is illustrated in Figure 31: it was expected that the most favorable conditions would be the low speed – high descent angle conditions (typically 60 knots with descent angle higher than 6°).

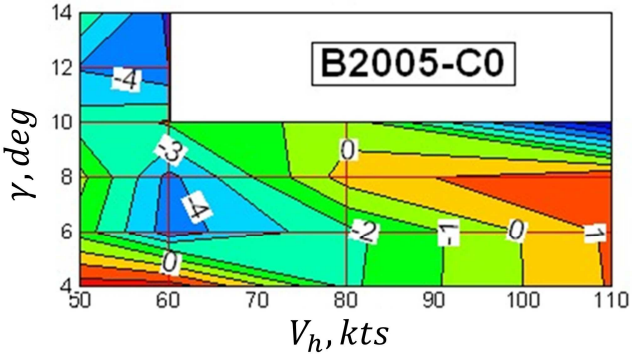

Figure 31: Final evaluation of the Blue Edge™. Contour plot of noise gains with respect to the C0 reference blade.

The feasibility of ERATO blade on the H155 helicopter was studied as soon as the interest of the fore-aft swept shape was confirmed by the results of the wind tunnel tests. The first studies showed instability of the blade for rotational speeds higher than the nominal one. The aeroelastic optimization of this kind of blades was difficult because of important backward offset. Indeed, it is of common usage to adapt the stiffness's and polar inertias with an adequate stacking of fabrics composing the structure of the blade. However, with this kind of geometry, most of the matter is found behind the lift center, therefore the centers of gravity, elastic and torsion are in a position ready to generate important couplings between the flapping and torsion modes. Although efforts were made to decrease the polar inertia of the backward swept area and to minimize the offsets of these centers compared to the lift center, this was not sufficient to have an acceptable margin with the phenomenon of instability. For the project of Blue Edge™ blade, the design of this zone was fundamental to improve this situation.

The requirements of design set out again from the same needs: to minimize the polar inertia of the backward offset by maintaining the torsion mode above 4/rev. Obtaining a product more mature and ready with the serial production, it was asked to make a blade design with the techniques of the state of the art, to minimize the increase of weight and the manufacturing costs. Consequently, the studied concept was to optimize the position of the center of gravity of the backward offset, to be closest to the total lift center. The way chosen was to avoid adding ballast while centering by counterweights but rather reducing to the maximum the backward area by reorganizing the placement of the components of the blade tip.

Usually, the spar of the blade, located in the leading edge, makes it possible to center the structure around the lift center while ensuring the hold of the centrifugal load and to bring an important bending stiffness. Preserving this principle in the zone of offset did not make sense because the angle of the swept edge is not aligned with the centrifugal force. It is of use to place the balancing system in the tip of the blade for a better effectiveness. By putting it in the zone behind the leading edge, it enables also to center this part of the blade correctly. To sustain in an optimal way the centrifugal load, the unidirectional glass fiber rovings of the spar were divided into two distinct ways at the beginning of the inboard swept zone. A part of the spar preserved its usual path while remaining in the leading edge and second was prolonged in a rectilinear way up to the balancing system. This structure with double spar, reinforced by carbon fabrics reinforcement, concentrates the matter at the good place with providing an optimal path for the efforts, Figure 32.

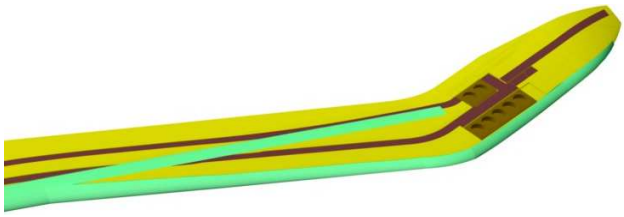

Figure 32: Blade structure with double spar.

This structural design is well visible during the manufacturing of the blades, Figure 33. To validate this solution, a section of this part of the blade was tested in fatigue, Figure 34.

Figure 33: Molded structure of the experimental Blue Edge™ blade.

Figure 34: Fatigue test on double swept area.

Solicited by multi-axial efforts, it passed the levels of vibratory fatigue successfully. Measurements from flight tests confirmed the good distribution of the constraints in the structure and confirmed the margins of resistance. The fore-aft swept shape was a challenge for the technological design of the blade. This technological definition has been patented (Ref. 33) and became a reference in the state of the art of the design of Blue Edge™-type blades, from which H160's main rotor blades were derived.

VALIDATION OF CONCEPT AT FULL-SCALE

The newly designed full-scale blade first flew on an H155 Dauphin demonstrator aircraft in Summer 2007, Figure 35. Detailed results of the extensive flight test campaign were previously highlighted in Refs. 31 and 34. During the more than 75 flight hours conducted within the test program, the full flight envelope was explored and specific attention was paid to performance, loads, airframe vibrations, and in particular to a thorough acoustics assessment.

Figure 35: Flight Tests of H155 Demonstrator with the Blue Edge™ Optimized Rotor.

The inflight validation of the concept was acquired by first confirming that the aircraft performances were in line with expectations (gains in HOGE and same power in level flight compared to the serial H155 straight blade). This was an important confirmation step since the original ERATO blade design had been modified in order to improve hover performance.

A large part of the validation also involved assessing the loads and vibrations. Pitch rod static loads were found to be lowered with the new blade and dynamic loads proved to be slightly increased at low reduced weight and slightly increased at high reduced weight. Airframe vibrations were also confirmed to be slightly lower with the new blades.

Since improved acoustics in approach was the main driver for the new blade, a strong focus was given to validating this aspect of the design and gaining a deeper understanding of the physical mechanisms at play for reducing BVI noise through a double-swept planform. Indeed, a significant portion of the flight test program was dedicated to assessing noise using advanced measurement means.

A first assessment was done using near-field microphones attached to the airframe. This allowed covering the whole flight envelope in a reduced time in order to obtain comparative results of the two blade shapes in the same atmospheric conditions. The expected noise reduction was thus quickly confirmed in a qualitative manner, and it was noted that impulsive noise was mostly eliminated from a large portion of the flight envelope (Figure 36). This feature offers greater capability for developing noise abatement procedures which use moderate descent angles and deceleration rates.

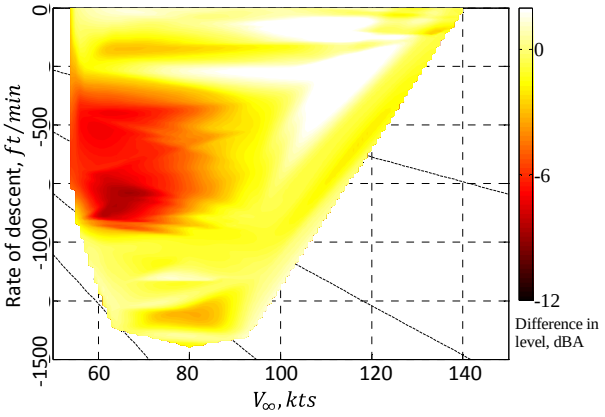

Figure 36: Difference between near-field A-weighted sound pressure levels for the two rotors (negative values where the reference rotor is louder), from Ref. 34.

Following the near-field tests, an extensive flight testing campaign was performed using a seven-microphone transversal ground array and focusing on providing a deeper analysis of the noteworthy features previously measured. The flights were of course performed with both the reference and Blue Edge™ rotors during successive days, ensuring again consistent ambient conditions. The tests with ground microphones not only allowed quantifying the operational noise reductions, but also were used to assess the directivity patterns associated with the two rotors.

The analysis focused on the flight conditions which showed the most differences between the straight blades and the Blue Edge™ blades. This was a descent at 60 kts with an 8° glideslope. In this condition, noise reductions of close to 5 EPNdB were measured close to the centerline, Figure 37. The analysis showed that this noise reduction was directly linked to a reduction of BVI noise. Interestingly, retreating side noise reductions were more significant than on the advancing side.

Further investigations of the measurements and additional computations using an acoustic solver coupled to a freewake code allowed to confirm that the blade's backward sweep was very efficient in shifting the directivities more towards the advancing side of the blade, to observers directly to the side of the aircraft. These observer positions are quite beneficial to noise reductions as highlighted in Ref. 34. Noise footprint assessments also shown in Ref. 34 illustrate the fact that the significant gains measured on the centerline and retreating side of the aircraft provide significant reductions in the surface area exposed to the loudest noise contours, which highlights the high potential of this rotor for community noise mitigation.

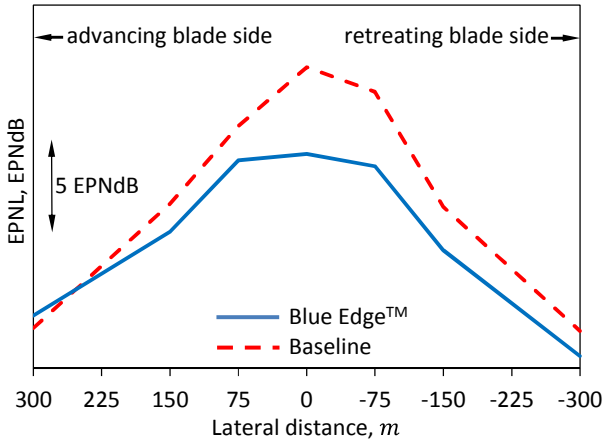

Figure 37: EPNL as a function of lateral distance for the baseline and the Blue Edge™ rotor, from Ref. 34.

CONCLUSIONS

The Blue Edge™ rotor blade is an excellent example of technology transfer from fundamental research to industrial application. After numerical optimization of the blade geometry using state-of-the-art comprehensive codes and structural design optimization to address aeroelastic issues, Mach-scaled model rotor blades were built and tested in large-scale wind tunnels. The results validated numerical predictions and industry took over the design for adaptation and further optimization with respect to industrial application. The major conclusions are:

- State-of-the-art comprehensive codes completed by high-order aerodynamic models (CFD) can successfully be employed for aero-acoustical optimization of rotor blades with respect to BVI noise reduction.
- Mach-scale models are invaluable to make a reliable proof of the design and generate data for a deep understanding of the physics involved.
- Based on fundamental work performed by ONERA and DLR within the ERATO project, Airbus Helicopters, together with ONERA, continued research and development with the aim of industrial application.
- Special attention was first given to further aerodynamic refinements of the blade tip for improvement of hover performance with respect to figure of merit, modifying the twist distribution and introducing anhedral.
- Special attention was given to the aeroelastic tailoring of the blade to assure structural integrity, leading to a double spar design.

- The results were confirmed by industry during flight tests, validating the transferability of model-scale wind tunnel tests to full-scale application.

The ERATO research project is a good example of efficient collaboration between the research and industrial worlds. Indeed, this very innovative blade design was initially conceived and tested using a wide array of the most advanced means, and then successfully adapted and flight tested at full-scale on a Dauphin demonstrator aircraft. This research has allowed demonstrating the maturity of the technology in time to allow the prototype of the Dauphin successor (the H160, Figure 38), to successfully launch its flight test campaign with the Blue Edge™ blades.

Figure 38: Flight testing trials of an Airbus Helicopters H160 prototype (©T. Rostang).

Author contact:
Philippe Beaumier philippe.beaumier@onera.fr
Berend G. van der Wall berend.vanderwall@dlr.de
Christoph Kessler christoph.kessler@dlr.de
Yves Delrieux yves.delrieux@onera.fr
Marc Gervais marc.gervais@airbus.com
Jean-François Hirsch jean-francois.hirsch@airbus.com
Kurt Pengel kurt.pengel@dnw.aero
Pascal Crozier pascal.crozier@onera.fr

ACKNOWLEDGMENTS

The following people are deeply acknowledged for their scientific contribution at different steps of this research: Jean Prieur, Patrick Gardarein, Arnaud Le Pape (all from ONERA), Wolf Splettstößer, Markus Raffel and the rotor test team (all from DLR), Reinert Müller (from FIBUS for support regarding the FCM technology and data evaluation). The test teams of DNW and S1MA wind tunnels are acknowledged for their support during the tests. The authors thank the French DGAC for their financial support to the ERATO, Blue-Edge and Shanel projects.

REFERENCES

[1] Kessler, Ch., "Helicopter emergency medical service: motivation for focused research," *CEAS Aeronautical Journal*, Vol. 6, (3), Aug. 2015, pp. 337-394. doi 10.1007/s13272-015-0157-0.

[2] Hirschberg, M., "Investing in Tomorrow`s Civil Rotorcraft," *Vertiflite*, Vol. 60, (4), July/Aug. 2014, pp. 4-5.

[3] Mooreman, R. W., "Helicopter Noise: The People's Perspective – Los Angeles County," *Vertiflite*, Vol. 60, (6), Nov./Dec. 2014, pp. 14-18.

[4] Mooreman, R. W., "Helicopter Noise: The People's Perspective – Long Island and Chicago," *Vertiflite*, Vol. 61, (1), Jan./Feb. 2015, pp. 28-30.

[5] Mooreman, R. W., "Noise in the Parks," *Vertiflite*, Vol. 61, (2), Mar./Apr. 2015, pp. 34-38.

[6] Kessler, Ch., "Active Rotor Control for Helicopters: Motivation and Survey on Higher Harmonic Control," *CEAS Aeronautical Journal*. Vol. 1, (1-4), Sept. 2011, pp. 3-22. doi: 10.1007/s13272-011-0005-9.

[7] Splettstoesser, W. R., Kube, R., Wagner, W., Seelhorst, U., Boutier, A., Micheli, F., Mercker, E., and Pengel, K., "Key Results From a Higher Harmonic Control Aeroacoustic Rotor Test (HART)," *Journal of the American Helicopter Society*, Vol. 42, (1), Jan. 1997, pp. 58-78.

[8] Yu, Y. H., "Rotor Blade-Vortex Interaction Noise," *Progress in Aerospace Sciences*, Vol. 36, (2), Feb. 2000, pp. 97-115. doi: 10.1016/S0376-0421(99)00012-3.

[9] Spiegel, P, and Rahier, G., "Theoritical study and prediction of BVI noise including close interactions," American Helicopter Society Technical Specialists' Meeting on Rotorcraft Acoustics and Fluid Dynamics, Philadelphia, PA, Oct. 15-17, 1991.

[10] van der Wall, B. G., Burley, C. L., Yu, Y. H., Richard, H., Pengel, K., and Beaumier, P., "The HART II Test-Measurement of Helicopter Rotor Wakes," *Aerospace Science and Technology*, Vol. 8, (4), Feb. 2004, pp. 273–284. doi:10.1016/j.ast.2004.01.001.

[11] N.N., "Environmental Protection, Volume I Aircraft Noise," Annex 16 to the Convention on International Civil Aviation, 6th Edition, ISBN-13: 978-92-9231-837-6, July 2011.

[12] Web-Site of EASA on Noise Type Certificate-Approved Noise Levels: www.easa.europa.eu/document-library/noise-type-certificates-approved-noise-levels.

[13] Leverton, J. W. and Pike, A. C., "Helicopter Noise – What is Important from a Community Prospective," American Helicopter Society 63rd Annual Forum Proceedings, Virginia Beach, VA, May 1-3, 2007.

[14] Hampson, M., "OEM Perspectives on Noise," *Vertiflite*, Vol. 60, (1), Jan./Feb. 2014, pp. 18-23.

[15] Spiegel, P., Guntzer, F., Le Duc, A., and Buchholz, H., "Aeroacoustic Flight Test Data Analysis and Guidelines for Noise-Abatement-Procedure Design and Piloting," 34th European Rotorcraft Forum Proceedings, Liverpool, UK, Sept. 16-19, 2008.

[16] Kessler, Ch., "Active Rotor Control for Helicopters: Individual Blade Control and Swashplateless Rotor Designs," *CEAS Aeronautical Journal*. Vol. 1, (1-4), Sept. 2011, pp. 23-54. doi: 10.1007/s13272-011-0001-0.

[17] Friedmann, P. P., "On-Blade Control of Rotor Vibration, Noise, and Performance: Just Around the Corner?" The 33rd Alexander Nikolsky Honorary Lecture. *Journal of the American Helicopter Society*, Vol. 59, (4), pp. 1-37, Oct. 2014. doi:10.4050/JAHS.59.041001.

[18] Crozier, P., Leconte, P., Delrieux, Y., Gimonet, B., Le Pape, A., and Mercier des Rochettes, H., "Wind Tunnel Tests of a Helicopter Rotor with Active Flaps," 32nd European Rotorcraft Forum, Maastricht, Netherlands, Sept. 12-14, 2006.

[19] Delrieux, Y., Le Pape, A., Leconte, P., Crozier, P., Gimonet, B., and Mercier des Rochettes, H., "Wind-Tunnel Assessment of the Concept of Active Flaps on a Helicopter Rotor Model", American Helicopter Society 63rd Annual Forum Proceedings, Virginia Beach, VA, May 1-3, 2007.

[20] Prieur, J. and Splettstoesser, W. R., "ERATO: an ONERA DLR Cooperative Programme on Aeroacoustic Rotor Optimisation," 25th European Rotorcraft Forum, Rome, Italy, Sept. 14-16, 1999.

[21] Splettstoesser, W. R., Prieur, J., Pahlke, K., Schultz, K.-J., van der Wall, B. G., Delrieux, Y., Gardarein, P., Geoffroy, P., and Leconte, P., "Main Phase of the ERATO Cooperation on Aeroacoustic Rotor Optimization." DLR Internal Report, DLR-IB 129-97/10, Braunschweig, Germany, 1997.

[22] Splettstoesser, W. R., Schultz, K.-J., Buchholz, H., van der Wall, B. G., Junker, B., Wagner, W., Mercker, E., and Pengel, K., "ERATO Rotor Validation Test in the DNW - Documentation and Representative Results," DLR Internal Report, DLR-IB 129-99/30, Braunschweig, Germany, 1999.

[23] Splettstoesser, W. R., van der Wall, B. G., Junker, B., Schultz, K.-J., Beaumier, P., Delrieux, Y., Leconte, P., and Crozier, P., "Wind Tunnel Test and Proof of Design for an Aeroacoustically Optimized Rotor," 25th European Rotorcraft Forum, Rome, Italy, Sept. 14-16, 1999.

[24] Müller, R.H.G., Pengel, K., and van der Wall, B. G., "Blade Deflection measurement at the Low Noise ERATO Rotor," 26th European Rotorcraft Forum, The Hague, Netherlands, Sept. 26-29, 2000.

[25] Delrieux, Y., Prieur, J., Costes, M., Gardarein, P., Beaumier, P., des Rochettes, H.M., Leconte, P., Crozier, P., Splettstoesser, W. R., van der Wall, B. G., Junker, B., Schultz, K.-J., Mercker, E., Pengel, K., Philippe, J. J., and Gmelin, B., "The ONERA-DLR Aeroacoustic Rotor Optimisation Programme ERATO: Methodology and Achievements," American Helicopter Society Aerodynamics, Acoustics, and Test and Evaluation Technical Specialists Meeting, San Francisco, CA, Jan. 23-25, 2002.

[26] Beaumier, P., and Bousquet, J.-M., "Applied CFD for Analysing Aerodynamic Flows Around Helicopters, " 24th International Congress of the Aeronautical Sciences (ICAS2004), Yokohama, Japan, Aug. 29-Sept. 3, 2004.

[27] Beaumier, P., and Delrieux, Y., "Description and validation of the ONERA computational method for the prediction of blade-vortex interaction noise," *Aerospace Science and Technology*, Vol. 9, (1), Jan. 2005, pp. 31–43.

[28] Le Pape, A., and Beaumier, P., "Numerical optimization of helicopter rotor aerodynamic performance in hover," *Aerospace Science and Technology*, Vol. 9, (3), April 2005, pp. 191–201.

[29] Le Pape, A., "Numerical Aerodynamic Optimization of Helicopter Rotors: Multi-Objective Optimization in Hover and Forward Flight Conditions," 31st European Rotorcraft Forum, Florence, Italy, Sept. 13-15, 2005.

[30] León, E.R., Le Pape, A., Désidéri, J.-A., Alfano, D., and Costes, M., "Concurrent Aerodynamic Optimization of Rotor Blades Using a Nash Game Method," 69th Annual Forum of the American Helicopter Society Proceedings, Phoenix, AZ, May 21-23, 2013.

[31] Rauch, P., Gervais, M., Cranga, P., Baud, A., Hirsch, J.-F., Walter, A., and Beaumier, P., "Blue Edge™: The Design, Development and Testing of a New Blade Concept," 67th Annual Forum of the American Helicopter Society Proceedings, Virginia Beach, VA, May 3-5, 2011.

[32] Rahier, G., and Prieur, J., "An Efficient Kirchhoff Integration Method for Rotor Noise Prediction Starting Indifferently from Subsonically or Supersonically Rotating Meshes." American Helicopter Society 53rd Annual Forum Proceedings, Virginia Beach, April 29-May 1, 1997.

[33] Hirsch, J.-F., and Rochegude, B., "Rotor blade provided with radial section and at least one arrowed section before and/or after," European Patent EP1961658, 2008.

[34] Gervais, M., and Gareton, V., "Analysis of Main Rotor Noise Reduction Due to Novel Planform Design – The Blue Edge™ Blade," 37th European Rotorcraft Forum, Gallarate, Italy, Sept. 13-15, 2011.